ACS central science

Research Article

http://pubs.acs.org/journal/acscii

Ultrahigh Surface Area Three-Dimensional Porous Graphitic Carbon from Conjugated Polymeric Molecular Framework

John W. F. To,[†,‡] Zheng Chen,[†,‡] Hongbin Yao,[§] Jiajun He,[∥] Kwanpyo Kim,[†,⊥] Ho-Hsiu Chou,[†] Lijia Pan,[#] Jennifer Wilcox,[∥] Yi Cui,[§,¶] and Zhenan Bao*[,†]

[†]Department of Chemical Engineering, [§]Department of Materials Science and Engineering, and [∥]Department of Energy Resources Engineering, Stanford University, Stanford, California 94305, United States

[⊥]Department of Physics, Ulsan National Institute of Science and Technology (UNIST), Ulsan 689-798, Korea

[#]National Laboratory of Microstructures (Nanjing), School of Electronic Science and Engineering, Nanjing University, Nanjing 210093, China

[¶]Stanford Institute for Materials and Energy Sciences, SLAC National Accelerator Laboratory, Menlo Park, California 94205, United States

Supporting Information

ABSTRACT: Porous graphitic carbon is essential for many applications such as energy storage devices, catalysts, and sorbents. However, current graphitic carbons are limited by low conductivity, low surface area, and ineffective pore structure. Here we report a scalable synthesis of porous graphitic carbons using a conjugated polymeric molecular framework as precursor. The multivalent cross-linker and rigid conjugated framework help to maintain micro- and mesoporous structures, while promoting graphitization during carbonization and chemical activation. The above unique design results in a class of highly graphitic carbons at temperature as low as 800 °C with record-high surface area (4073 $m^2 g^{-1}$), large pore volume (2.26 cm^{-3}), and hierarchical pore architecture. Such carbons simultaneously exhibit electrical conductivity >3 times more than activated carbons, very high electrochemical activity at high mass loading, and high stability, as demonstrated by supercapacitors and lithium−sulfur batteries with excellent performance. Moreover, the synthesis can be readily tuned to make a broad range of graphitic carbons with desired structures and compositions for many applications.

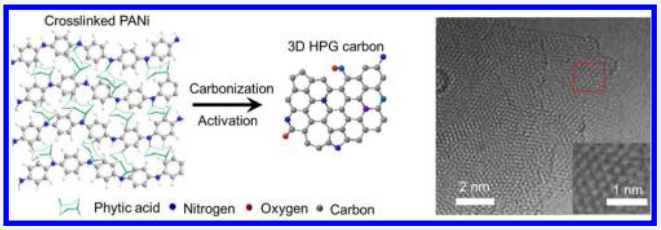

INTRODUCTION

High surface area porous carbon materials are of great technological importance due to their diverse functionalities and excellent physical/chemical robustness. Their high electronic conductivity, large surface area, and good chemical and electrochemical stability are of particular interest for electrochemical energy storage devices, such as electrochemical capacitors (or supercapacitors) and batteries.[1] Fundamentally, the performance of such devices mainly depends on the capability of carbon materials to interact with ions and to transport electrons. For example, an ideal supercapacitor carbon material requires high conductivity for electron transport, high surface area for effective ion adsorption/desorption, and suitable pore architecture for rapid access of ions from electrolyte solution to the carbon surface. Traditional porous carbon materials, such as activated carbons (ACs), have high surface area (up to 3000 m^2/g), but their large pore tortuosity and poor pore connectivity severely limit electrolyte ion transport to the surface.[2] Furthermore, they are generally synthesized from coal or biomass (e.g., coconut shell, rice husk) containing a large amount of impurities. As a result, extensive purification is needed to achieve high-quality supercapacitor-grade AC, which substantially increases the cost.[3] Soft or hard templates can be used to prepare mesoporous carbons to achieve better pore size control and tunable pore connection; however, complicated and costly synthesis is required, prohibiting their practical applications.[4]

Porous graphitic carbons, such as three-dimensional (3D) porous graphene network, are attracting increasing interest owing to their high intrinsic electronic conductivity and large surface area.[5] However, bulk graphene powder made from random stacking of individual sheets often suffers from severe aggregation, which dramatically decreases its surface area, pore connectivity, and electronic conductivity, leading to moderate charge storage performance.[5a] While some specially designed 3D porous graphene networks[6] show good pore connectivity and conductivity, large-scale and low-cost fabrication of such graphene networks remains a challenge. The general strategy toward the above-mentioned graphene networks is to use graphene oxides (GOs) as building blocks. However, making conductive graphene from GO building blocks (normally by Hummer's method[7]) requires strong oxidative and subsequently reductive chemicals, which is unfavorable for large-scale

Received: April 15, 2015
Published: May 18, 2015

DOI: 10.1021/acscentsci.5b00149
ACS Cent. Sci. 2015, 1, 68−76

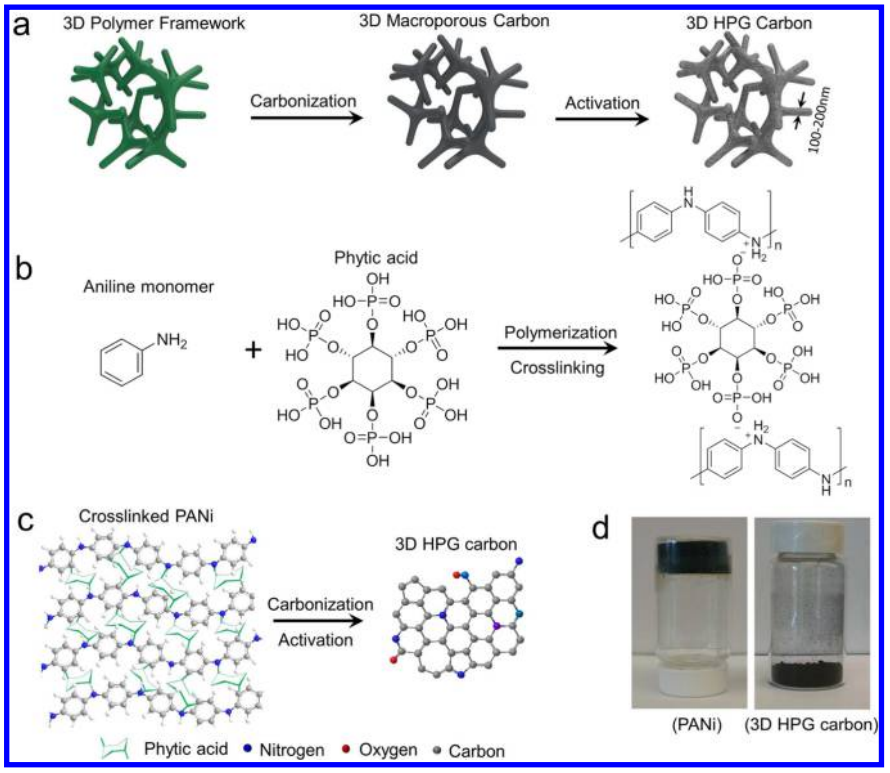

Figure 1. Synthesis of 3D HPG. (a) Schematic synthetic preparation of 3D HPG carbon network from the nanostructure polymer molecular framework. The phytic acid helps to maintain the 3D structure, prevent pore collapse, and retain volatile low molecular weight species during carbonization and activation processes. (b) Illustration of the chemical synthesis of PANi hydrogel in which the phytic acid acts as both dopant and cross-linker. (c) Illustration of transformation of phytic acid cross-linked PANi (left) into doped graphene-like carbon sheets (right). (d) A digital photograph showing the phytic acid cross-linked PANi aerogel (left) and the 3D HPG carbon (right) made from 700 °C carbonization with 800 °C activation. A typical total yield is 30 wt % from polymer to 3D HPG carbon.

production. In this context, efficient synthesis of 3D interconnected graphitic carbon networks remains highly desired.

Herein, we report a scalable synthesis toward low-cost and low-temperature synthesis of 3D porous graphitic carbon networks with ultrahigh surface area and hierarchically interconnected pore architecture. Our strategy is using a 3D cross-linked precursor from a conjugated polymeric molecular framework without using any sacrificial templates (Figure 1a). As shown in Figure 1b,c, we began with the synthesis of a cross-linked conjugated polymeric molecular framework, which can be readily converted into porous carbon simply by thermal annealing (carbonization). A subsequent chemical activation process at a temperature as low as 800 °C further increases the surface area and porosity, leading to a 3D hierarchically porous graphitic (HPG) carbon framework with high surface area (up to 4073 $m^2 g^{-1}$), large pore volume (up to 2.26 $cm^3 g^{-1}$), high electronic conductivity (>3 times higher than typical ACs), and good pore connectivity. The resulting HPG carbon materials showed unprecedented energy storage capacity and rate capability compared with previously reported porous carbons, enabling high mass loading supercapacitors and highly stable lithium−sulfur batteries. Dai and co-workers reported on synthesis of N-doped carbon using our PANi hydrogel precursor for electrocatalysis applications during this manuscript preparation.[8] However, their synthesis did not include chemical activation, the carbonization required 1000 °C, and the resulting carbon had a low surface area of 1663 $m^2 g^{-1}$.

RESULTS

Synthesis of Ultrahigh Surface Area and Highly Graphitic Framework at Low Temperature. Our polymer network is termed "molecular framework" because of its rigid and cross-linked structure. The rigid conjugated polymer backbone, PANi, was formed in the presence of a cross-linker. The hydrogel network is readily formed upon mixing the monomer, oxidizing agent, and a cross-linker as we previously reported[9] (see experiments). After water removal by freeze-drying, the hydrogel was converted into an aerogel, which maintained the original macroscopic structure of the polymer network (Figure 1d). Seen from the scanning electron microscopic (SEM) image (Figure S1), the dried polymer shows interconnected coral-like nanofibers with diameters of about 100−200 nm.

Phytic acid is selected as the cross-linker for two reasons: (1) It contains six phosphoric acid groups, which electrostatically associate with protonated aniline to cross-link the entire network, giving rise to the 3D macroscopic structure of a molecular framework. Unlike soft templates which are selected for their low decomposition temperature <300 °C, the degradation temperature of phytic acid is relatively high, ~380 °C, which prevents pore collapsing during carbonization. (2) As phytic acid is carbonized, the *in situ* formed organophosphates were reported to generate a polymeric layer through the formation of phosphate linkages that connect and further cross-link polymer fragments.[10] This can help to effectively retain the more volatile lower molecular weight species. Indeed, we obtained a high carbon yield (~50 wt %), which is more than twice that of carbonization of biomass.[11]

DOI: 10.1021/acscentsci.5b00149
ACS Cent. Sci. 2015, 1, 68−76

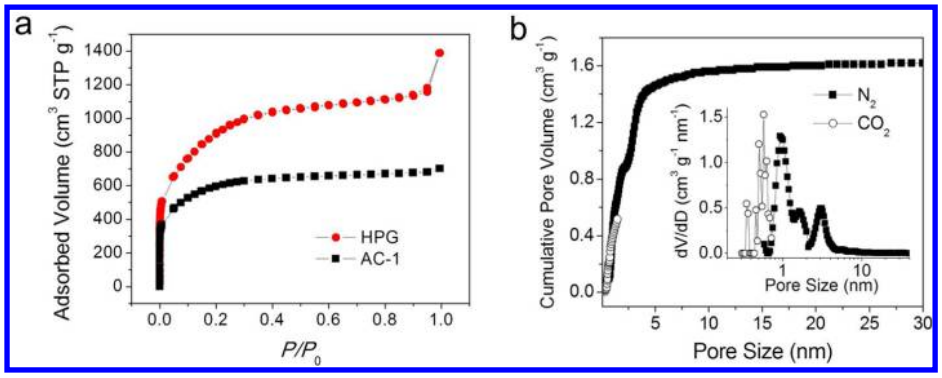

Figure 2. Porosity and composition of 3D HPG carbon. (a) N_2 adsorption/desorption isotherm of HPG carbon, clearly showing the hierarchically porous structure. The significant N_2 uptake at a relative pressure (P/P_0) below 0.01 is a typical characteristic of micropores. The continuous N_2 uptake at P/P_0 between 0.05 and 0.3 is attributed to N_2 adsorption in the mesopores. The N_2 uptake with a relatively flat region followed by a rapid increase at P/P_0 of 0.9 suggests the existence of large mesopores and macropores. Isotherms of a commercial high surface area AC (AC-1, for supercapacitor application with high S_{BET} of 1970 m^2 g^{-1}) are also provided for comparison. No obvious continuous N_2 uptake at P/P_0 between 0.05 and 0.3 indicates the lack of sufficient mesopores. (b) Cumulative pore volume and pore size distribution (inset) for N_2 and CO_2 adsorption. Pore size distribution was calculated by nonlinear density functional theory (NLDFT) by assuming slit pore geometry for micropores and cylindrical geometry pore for mesopores.

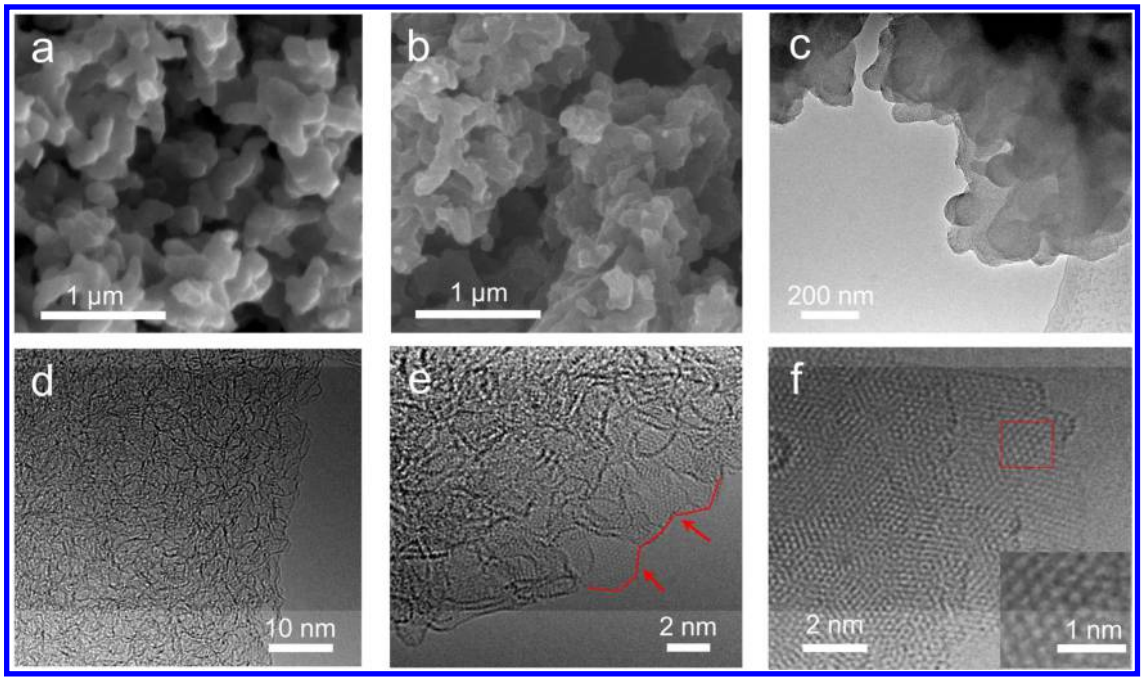

Figure 3. Structure and morphology of 3D HPG carbon. (a) SEM image of carbonized PANi polymer at 700 °C. (b, c) SEM and TEM images showing the macroscopic network (primary) and macroporous feature of the 3D HPG carbon after activation at 800 °C. (d) TEM image revealing the mesoporous structure of the graphitic network (secondary) after 800 °C activation. (e) HR-TEM image showing the network of graphene sheets, which have a typical lateral dimension of a few nanometers. (f) HRTEM showing a relatively large graphene sheet with clearly ordered hexagonal carbon atom packing. Inset shows the zoomed-in image at the box in panel f.

At even higher temperatures (>450 °C), cyclization and condensation reactions lead to increases in aromaticity and size of the polyaromatic units, enabled by the scission of P−O−C bonds.[10a] Extensive growth of these aromatic units or "embryonic" graphene layers in the carbonized polymer can be observed in transmission electron microscopic (TEM) images (Figure S2). A subsequent chemical activation process by mixing the above graphitized carbon with potassium hydroxide (KOH) followed by a heat treatment at 800 °C further increases the porosity and surface area. After activation, a typical overall carbon yield (vs mass of polymer) of ∼30 wt % can be achieved. By comparison, common carbon yield of commercial ACs made from activation of biomass at similar temperature is only ∼8%.[12]

The surface area and pore structure of the polymer-derived porous graphitic carbon can be readily tuned by adjusting the synthetic conditions, such as annealing temperature and activation conditions (Table S1). For example, by increasing carbonization temperature from 400 to 900 °C, BET (Brunauer−Emmett−Teller) surface area (S_{BET}) can be increased from 20 m^2 g^{-1} to 423 m^2 g^{-1}. At the same time, the pore volume (V_{Ar}, measured with argon) can be increased from 0.04 to 0.38 cm^3 g^{-1}. Subsequent chemical activation of these carbons can further enhance S_{BET} to as high as 4073 m^2 g^{-1} and V_{Ar} to 2.26 cm^3 g^{-1}. This effect may have contributions

DOI: 10.1021/acscentsci.5b00149
ACS Cent. Sci. 2015, 1, 68−76

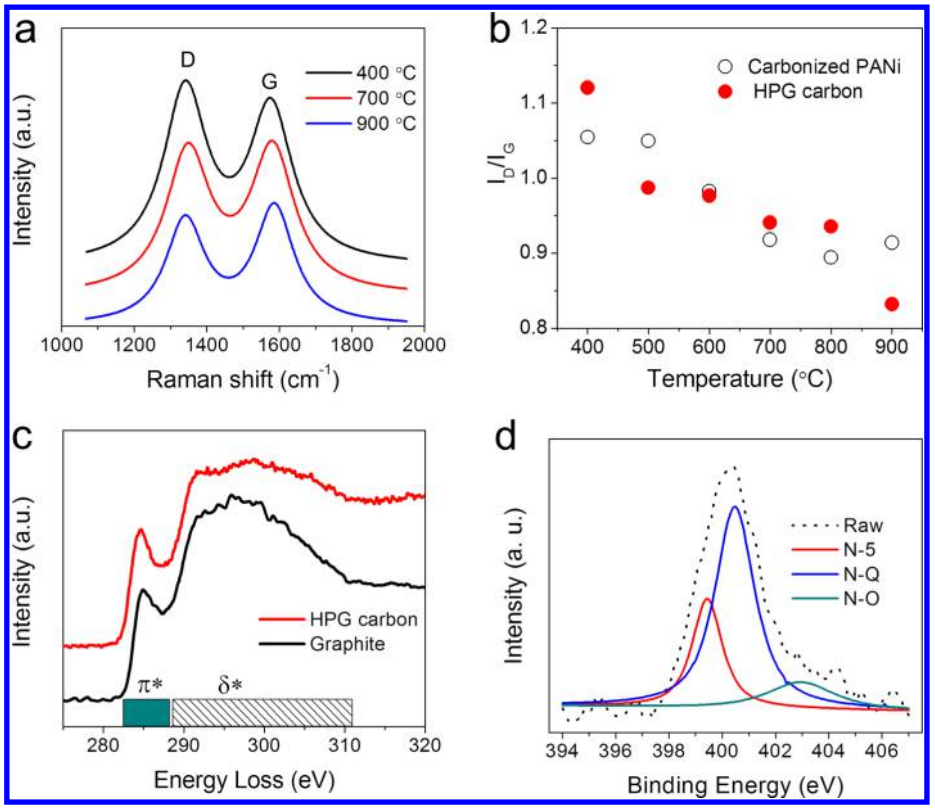

Figure 4. (a) Raman spectra of 3D HPG carbons made from activation of carbonized PANi aerogel at 400, 700, and 900 °C. (b) Summary of I_D/I_G for carbonized PANi and 3D HPG carbons from different carbonization temperatures. (c) Comparison of EELS spectra of HPG carbon and graphite suggesting a large portion (~94% ± 5%) of sp^2 bonding in the HPG carbon. (d) N 1s XPS spectra indicating the existence of N dopants at different chemical environments in the carbon framework.

from the activation from phosphoric acid group and organophosphate moieties that are generated during decomposition of phytic acid. Note that the highest surface area attained is the sample with the lowest carbonization temperature (400 °C), and as the carbonization temperature increases to 900 °C while fixing the activation temperature and KOH/C ratio, S_{BET} first decreases and then increases. This confirms the unique role of phytic acid as a cross-linker and its effect in retaining the structural integrity at moderate temperature. Such high S_{BET} together with large V_{Ar} is the highest achieved among graphitic carbons.[6b,13] This value is even higher than that for the previously reported activated graphene (S_{BET} = 3100 m^2 g^{-1}, V_{Ar} = 2.14 cm^3 g^{-1}).[13a] We attribute this to the unique activation effect of phytic acid and the rigid carbon framework, which prevents pore collapsing.

Detailed pore structure was probed by N_2 adsorption/desorption techniques at 77 K (Figure 2a), which clearly showed the coexistence of micro-, meso-, and macropores of typical 3D HPG carbons. CO_2 adsorption/desorption isotherm at 273 K further revealed a steady increase of CO_2 uptake under low pressure (Figure S3). Figure 2b summarizes the cumulative pore volume and pore size distribution from N_2 and CO_2 adsorption. By comparison, a typical commercial high surface area AC (Figure 2a) only shows micropores with small peak pore size (~0.6 nm, Figure S4 and Figure S5) and moderate V_{Ar} (0.997 cm^3 g^{-1}). The existence of abundant meso-/macropores in the HPG carbon allows a better mass transport than for normal ACs with only micropores. The high flexibility of this synthetic approach makes it possible to achieve unprecedented performance for a wide range of applications, such as electrochemical energy storage.

Physical and Chemical Characterization of the HPG Carbon. The 3D HPG carbons synthesized at different carbonization temperatures share similar morphology and structure. Detailed microstructure characterization reveals their hierarchical architectures. Typical SEM (Figure 3a) and TEM images (Figure 3b) show the interconnected carbon framework (primary) with large pores (a few hundred nanometers) formed during the polymerization of PANi (Figure S1). Close examination of the carbon backbone shows a foamlike porous structure with small mesopores with pore sizes in the range of a few nanometers (Figure 3c). The observed filamentary carbon structure suggests that carbon sheets further intertwine into a continuous porous framework (secondary). High-resolution TEM (HRTEM) images (Figure 3d,e) further identify the interconnected graphene sheets with lateral dimensions of a few nanometers. The ordered hexagonal packing of the carbon atoms in graphene nanosheets can be clearly seen, suggesting a high degree of graphitization of the carbon framework. This porous graphitic structure highly resembles porous graphene derived from chemical activation of graphene oxide at the same temperature, which shows small graphene domains and abundant edge sites.[13a] Nevertheless, our HPG carbon shows good pore connectivity originated from the rigid 3D conjugated polymer network, which can prevent particle aggregation or layer-to-layer stacking. This HPG carbon structure is in sharp contrast to previously reported pyrolysis porous carbons, which mostly contain amorphous carbon at similar or even higher carbonization temperatures.[11b,14]

DOI: 10.1021/acscentsci.5b00149
ACS Cent. Sci. 2015, 1, 68−76

Raman spectroscopy further confirms the strong graphitization of all the 3D HPG carbons as featured by intensive G-bands at ~1590 cm^{-1} (Figure 4a). While graphitic structures were attained for all samples, the degree of graphitization increases with the increase of carbonization temperature. The D-band to G-band intensity ratio (I_D/I_G) was calculated to be 1.12, 0.94, and 0.83 for HPG carbon from PANi carbonized at 400, 700, and 900 °C, respectively (Figure 4b, Table S1), which is consistent with their different surface area and porosity. Even the maximum I_D/I_G is smaller than that of GO-derived activated graphene (~1.2) with a similar activation condition,[13a] indicating a higher degree of graphitization. However, due to the highly porous structure and overlap of small graphene domains, our 3D HPG samples show a weak 2D band (Figure S6). The amount of sp^2 carbon is further determined by comparing the π^* and σ^* bonding to a graphite standard with equivalent thickness by using electron energy loss spectroscopy. For example, the fraction of sp^2 carbon in HPG carbon (from 900 °C carbonization) was found to be as high as 94% (±5%, Figure 4c), assuming the graphite reference spectrum is 100%.[15] We note that this value may be underestimated due to the presence of abundant small graphene sheets (Figure 3d–b, Figure S7) in the filamentary network which can project more edge defects to electron beam, thus reducing the detected content of sp^2 carbon.

X-ray photoelectron spectroscopy (XPS) shows that typical HPG carbon contains C, N, and O dopants (Figure S8) but an undetectable amount of P. Elemental analysis further confirms that P content is below 1 ppm for sample carbonized at 700 °C. The N 1s core level spectrum (Figure 4d) suggests the presence of three types of nitrogen: pyrrolic nitrogen (N-5, 399.5 eV), quarternary nitrogen (N-Q, 400.6 eV), and oxides of pyridine-N peak (N-O, 402.9 eV). The N-5 (25 atom % for total N) originated from structure confinement and low molecular weight PANi produced from the rapid polymerization. The N-Q predominates (61 atom %) due to its highest thermal stability.[16] The existence of N-O (14 atom %) can be ascribed to the oxidizing environment of the activation process. The total N content of HPG carbon can be tuned from 0.55% to 2.33% depending on carbonization temperature (Table S1). Such development of doping in HPG carbon is also elucidated by analyzing the composition of PANi and carbonized PANi (Figure S9 and Figure S10).

Electrochemical Performance of HPG Carbon-Based Supercapacitors. The high surface area and 3D pore structure of the HPG carbon are favorable for electrode applications. In addition, the relatively small carbon particle size offers scalability and high flexibility for processing. Essentially, the HPG carbon-based electrodes can be easily fabricated on various substrates. For example, micropatterned electrodes can be directly spray coated on polyethylene terephthalate (PET) sheets, flexible polyimide films, or silicon wafers from an ink consisting of carbon suspension in ethanol (Figure 5a–c). Very thick electrodes (>100 μm) can be readily blade coated on metallic substrates (e.g., Ti, Al) using carbon slurry in *N*-methyl-2-pyrrolidone (Figure 5d). Since the carbon particles are composed of interconnected coral-like nanofibers, they provide electrodes with good mechanical flexibility. The resulting electrodes also possess high conductivity (~300 S m^{-1}), which is close to that of activated graphene (500 S m^{-1})[13a] and significantly higher than that of strutted graphene (1 S m^{-1})[17] and commercial ACs (10–100 S m^{-1}).[11b,18] Together with large active surface area, such electrodes hold great potential for supercapacitors, batteries, electrocatalysts, and other applications.

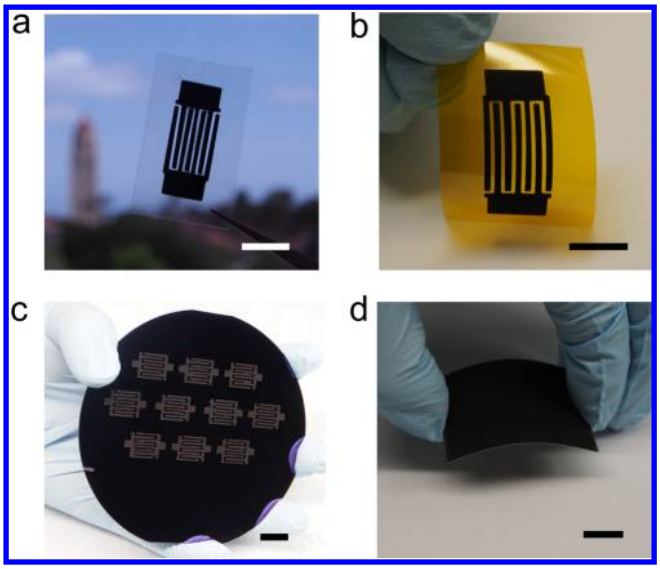

Figure 5. HPG carbon electrodes and supercapacitors fabricated on different substrates. (a) An interdigital supercapacitor made by spray coating HPG carbon ink on a gold-coated (50 nm) PET film. (b) A flexible supercapacitor with interdigital electrodes made by spray coating HPG carbon ink on an Al-coated (50 nm) Kapton polyimide film with 50 nm Al conducting layer. (c) Ten supercapacitors with interdigital electrodes fabricated at the same time on a silicon wafer using a removable PDMS (polydimethylsiloxane) mask. (d) A 4 cm × 5 cm size electrode (thickness of ~100 μm) made by blade coating HPG carbon slurry on a Ti substrate. Scale bar, 1 cm (a–d).

To evaluate supercapacitor performance, we used a conventional slurry coating method to fabricate electrodes. The devices showed high performance in both aqueous and organic electrolyte (Figure S11). For example, prototype devices based on HPG carbon maintained rectangular cyclic voltammetry (CV) curves even at a very high voltage sweep rate of 1000 mV s^{-1} in 0.5 M H_2SO_4 (Figure 6a), a feature observed only for ideal supercapacitors.[19] Typical galvanostatic charge/discharge profiles show linear curves with a small voltage (*IR*) drop, for example, only 0.014 V drop at a current density as high as 10 A g^{-1} (Figure 6b). This value is only 1/5 of the value for AC-1 (a commonly used supercapacitor carbon) and lower than that of the graphene thin film supercapacitor (0.018 V).[6b] Specific capacitance of the HPG carbon and typical commercial ACs at different current densities from 0.5 to 50 A g^{-1} are summarized in Figure 6c. The HPG carbon showed a capacitance of 225 and 162 F g^{-1} at a current density of 0.5 and 50 A g^{-1}, respectively, corresponding to a capacitance retention of 72%. By comparison, AC-1 maintained only ~44% of the initial capacitance (198 to 88 F g^{-1}) as current density increased from 0.5 to 50 A g^{-1}. Even for thin-film graphene,[6b] macro-/mesoporous graphene,[20] and 3D strutted graphene supercapacitors,[17] the capacitance retention was only ~50% as current density increased by the same magnitude. We note that the N dopant in our HPG carbon may have contributed to the measured capacitance due to pseudocapacitive effect.

The fast electrode kinetics was further confirmed using electrochemical impedance spectroscopy (EIS). A typical Nyquist plot of HPG carbon (Figure 6d) reveals a very low electrode series resistance (ESR, ~0.7 ohm), which is attributed to the highly graphitized porous network. The nearly vertical

DOI: 10.1021/acscentsci.5b00149
ACS Cent. Sci. 2015, 1, 68–76

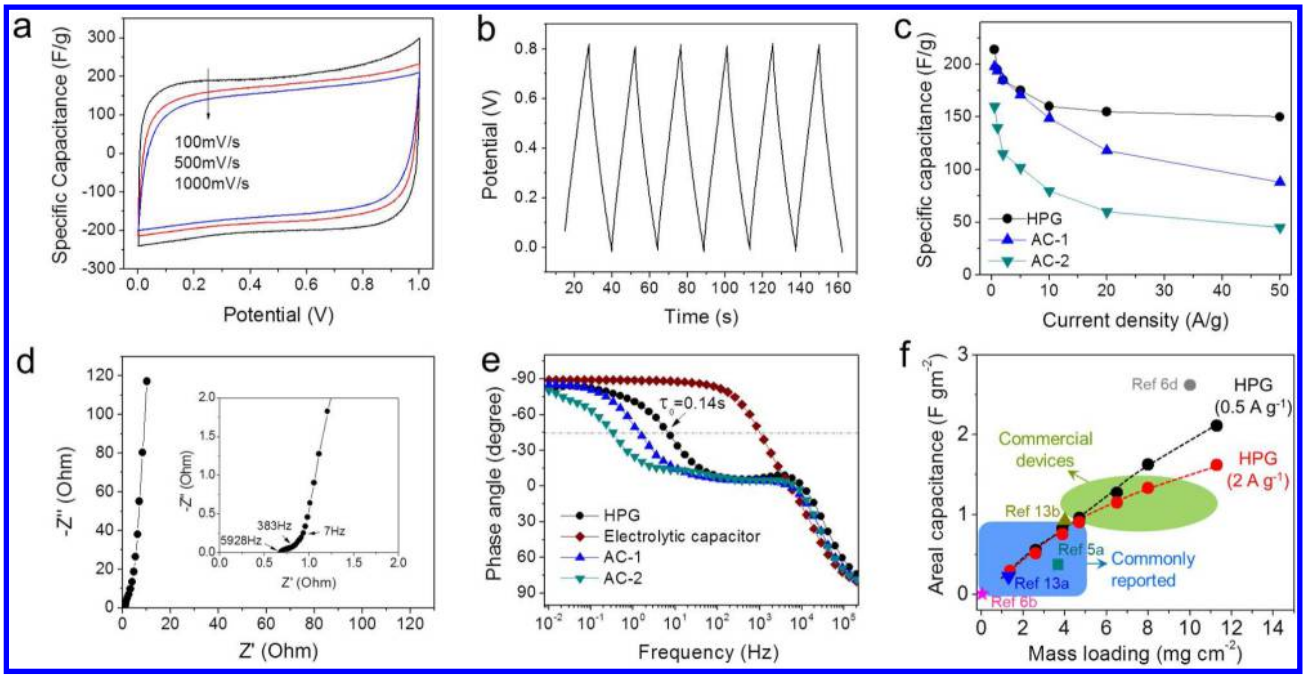

Figure 6. HPG carbon supercapacitor performance in 0.5 M H_2SO_4 aqueous electrolyte. (a) Representative CV curves of HPG carbon supercapacitors at scan rates of 100, 500, and 1000 mV s^{-1}. The mass loading of electrodes for CV measurement was ~1.5 mg cm^{-2}. (b) Typical galvanostatic charge/discharge curve of single HPG carbon electrode (in three-electrode cell) at a current density of 10 A g^{-1}. (c) Specific capacitance dependence on current density of supercapacitor electrodes made from different porous carbon. The HPG carbon shows higher capacitance and significantly better rate capability than ACs. (d) Nyquist plot of a symmetric supercapacitor device made from HPG carbon. Inset shows the high-frequency range. (e) Impedance phase angle versus frequency for one HPG carbon-based and two commercial AC-based supercapacitors. A commercial electrolytic capacitor was also compared. The characteristic frequency f_0 occurs at phase angle of 45° where resistive and capacitive impedance are equal. As expected, the electrolytic capacitor shows a high characteristic frequency f_0 of 1,000 Hz due to the absence of ion diffusion process. The f_0 occurs at ~7 Hz for HPG carbon, 1 Hz for AC-1, and ~0.1 Hz for AC-2. (f) Dependence of areal capacitance on mass loading of HPG carbon electrodes at current densities of 0.5 and 2 A g^{-1}. Commercial supercapacitors have an areal capacity of ~1 F cm^{-2}, while most of the recently reported high-performance electrodes have low or moderate areal capacity (<1 F cm^{-2}).

line displayed at low-frequency range further suggests an ideal capacitive behavior due to facile ion transport.[19] More clearly, Bode plots shown in Figure 6e compare the response times of different supercapacitors. For commercial ACs, the characteristic frequency (f_0) is on the order of 0.1−1 Hz.[6b] Remarkably, our HPG carbon devices show a high f_0 of ~7 Hz, which corresponds to a time constant τ_0 (=1/f_0) of only ~0.14 s. This value is also lower than that of activated graphene (~0.25 s),[6b] liquid-mediated dense graphene (0.51−3.85 s),[6c] and holey graphene framework (0.17−0.49 s).[6d] The short time constant is mainly due to the 3D interconnected hierarchically porous structure, which provides fast ion transport in the bulk electrodes.

Practical application of supercapacitors requires high active mass loadings to obtain large areal capacitances.[21] Our HPG carbon can be easily made on gram scale in powder form, and high mass loading electrodes can be readily attained. Owing to the effective porous conductive structure, the HPG carbon electrodes can retain ~83% of the initial capacitance (from 225 to 187 F g^{-1}) at 0.5 A g^{-1} as mass loading increased from 1 to 11 mg cm^2, which corresponds to an areal capacitance of 2.12 F cm^{-2} (Figure 6f). The areal capacity can still be maintained as 1.62 F cm^{-2} at a current density of 2 A g^{-1}. Such high areal capacitances and high rate capability meet the requirements for commercial supercapacitors (e.g., >1 F cm^{-2}). However, previously reported high-performance porous graphitic carbon electrodes could only achieve low/moderate mass loadings (<5 mg cm^{-2}) or are difficult for large-scale industry manufacturing.[6c,d]

In addition, the HPG carbon electrodes showed a highly stable cycling performance, with capacitance retention of 96% after 10,000 cycles at 5 A g^{-1} (Figure S12). The EIS measurement of prototype devices before and after cycling showed little change in ESR (Figure S13), which confirms the high electrochemical stability of our HPG carbon.

Electrochemical Performance of HPG Carbon for Li−S Batteries. In addition to supercapacitors, the HPG carbon can enable high-performance lithium−sulfur (Li−S) batteries owing to the aforementioned structure merits. One critical challenge for Li−S battery is to provide large conducting surface area for activating and trapping the insulating sulfur, lithium sulfide, and polysulfide species in electrodes. While a variety of porous carbons have been used for Li−S cathodes, they often show insufficient cycling stability and/or low sulfur mass loadings (<2 mg cm^{-2}) due to moderate surface area and lack of effective pore structure to keep active sulfur species and thus electrode activity.[1d,22] Again high mass loading could not previously be realized due to the poor conductivity of the carbon electrodes.

A schematic of the cell structure is shown in Figure S14. Charge/discharge voltage profiles of HPG carbon/polysulfide electrodes show a typical two-step discharging behavior (Figure 7a, Figure S15a).[23] The electrodes exhibit exceptional electrochemical activities. The initial discharge capacity (sulfur loading: 3.2 mg cm^{-2}) at a rate of C/5 was ~1270 mAh g^{-1}, approaching ~90% of the theoretical capacity (1466 mAh g^{-1},

DOI: 10.1021/acscentsci.5b00149
ACS Cent. Sci. 2015, 1, 68−76

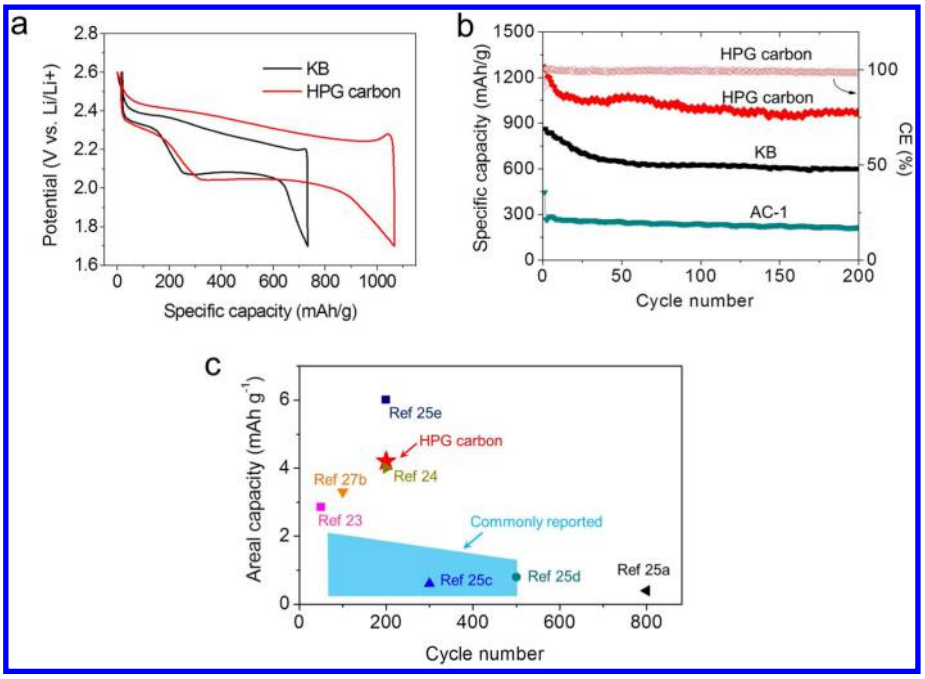

Figure 7. Electrochemical performance of 3D HPG carbon for Li–S batteries. (a) Charge/discharge voltage profiles at a *C*/5 current rate for HPG carbon/polysulfide and KB/polysulfide electrode after equilibrium, respectively. The discharging curve starts with plateaus at 2.4 and 2.05 V, while the charging curve displayed overlapped plateaus starting from 2.4 V. (b) Long-term cycling stability of HPG carbon/polysulfide (3.2 mg cm^{-2}), AC-1/polysulfide (2.56 mg cm^{-2}), and KB/polysulfide (1.28 mg cm^{-2}) electrodes, respectively. After initial activation, high coulombic efficiency (CE, ~99.8%) was maintained for HPG carbon electrode during all the cycles. (c) Comparison of areal capacity and cycling life between HPG carbon/sulfur electrodes and recently reported high-performance sulfur electrodes. Previously reported sulfur electrodes often had areal capacity of below 3 mAh g^{-1} and cycling lifetime of less than 200 cycles.

Li_2S_8 to Li_2S).[24] Accordingly, the areal capacity reached a value as high as 4.2 mAh cm^{-2}. A capacity of 920, 740, and ~600 mAh g^{-1} can be delivered at rate of 0.5*C*, 1*C*, and 2*C*, respectively (Figure S15b), indicating a high rate capability at a high mass loading. After initial equilibrium cycles, the electrodes can retain a high capacity of 980 mAh g^{-1} after 200 cycles (~80% of initial capacity) at *C*/5 (Figure 7b). The high specific capacity attained at high mass loading can be attributed to the effective hierarchically porous conductive architecture and the doping atoms of N and O for the strong Li_xS interaction that controls the formation of lithium sulfide species and maintains high active material utilization. This performance is superior to most porous carbon-based sulfur electrodes reported so far (<3 mAh cm^{-2}, < 200 cycles, Figure 7c).[23−25]

By comparison, control electrodes made from AC-1 (sulfur loading: 2.52 mg cm^{-2}) showed low capacity (<400 mAh g^{-1}). This might be due to the low electrical conductivity and poor electrolyte wetting and diffusion in the microporous AC particles. Similarly, electrodes made from carbon black (Kejten black, S_{BET} of 1200 m^2 g^{-1}) also showed a low initial capacity of 890 mAh g^{-1} even at a low sulfur loading (1.28 mg cm^{-2}). Moreover, such electrodes only retained a capacity of 600 mAh g^{-1} after 200 cycles. Their faster capacity drop can be ascribed to uncontrolled deposition of insulating sulfide species, which resulted in large inactive particles and loss of electrode activity.[26] In our HPG carbon electrodes, the ultrahigh surface area and polar doping atoms (N, O) provide more active sites for lithium sulfide deposition, and the interconnected framework can effectively maintain conductive pathways,[25e,27] thus providing high cycling stability. This is supported by EIS measurements (Figure S16), where the ESR of HPG carbon/polysulfide remains small during cycling. It is noted that cycling stability of over 500 cycles was only reported with sulfur mass loading of <1 mg cm^{-2}.[25a,c,d] However, making high mass loading electrodes always results in significantly decreased lifetime. Our high sulfur mass loading HPG carbon electrodes are therefore highly promising for practical applications.

DISCUSSION

The 3D HPG carbon framework outperforms other reported porous carbons, commercial activated carbon, and other 3D porous graphenes in terms of their electrochemical charge storage capability because of their highly graphitic structure with ultrahigh surface area, large pore volume, and interconnected pore architecture. Even though ACs with high S_{BET} of ~3000 m^2 g^{-1} have been reported, their electrochemical capacitance and rate capability were worse.[28] In our case, we also found that the best supercapacitive performance was not from the sample with the highest surface area. This is likely due to the more irregular pore structure that is unfavorable for mass transport.[28] Nevertheless, our versatile synthesis approach allows high structural tunability to achieve unprecedented electrochemical performance. For carbon black, there are no pores inside carbon particles, thus the total surface area is insufficient for supercapacitor application. Moreover, their particle size is so small (<100 nm) that contact resistance is very large especially for thick electrodes. This is even worse in Li–S batteries, where insulating polysulfide deposited on the particle surface can block the charge-transfer pathway easily. By comparison, the HPG carbon framework is composed of a 3D porous network of small graphene sheets and, thus, can simultaneously achieve high surface area, small carbon particle size, open pore structure, and good conductivity. As a result,

DOI: 10.1021/acscentsci.5b00149
ACS Cent. Sci. 2015, 1, 68−76

critical requirements are satisfied for high-performance electrodes: (i) efficient transport of ions and minimal electrolyte transport resistance, (ii) large electrode/electrolyte interface to provide a large number of active sites for redox reaction, thus enabling a high charge storage capacity, and (iii) graphitized carbon framework that ensures high electronic conductivity for efficient charge transfer and high chemical stability. These features together enable fast kinetics and low ESR, providing high rate capability for electrodes. Therefore, this class of porous graphitic carbons holds great promise for supercapacitors and Li−S batteries with high energy and high power density.

It is noted that a few other 3D porous graphene structures have been recently reported. For example, graphene networks can be made from a templated chemical vapor deposition (CVD) process followed by etching, but large-scale production using CVD remains challenging.[6a] While strutted graphene grown from a sugar blowing process can be potentially made in a large scale, its ultrahigh porosity (99.85%) and ultralow density (~3 mg cm^{-3}) make it challenging to fabricate devices with reasonable volumetric energy density.[17] Laser induction of commercial polymer was used to prepare 3D porous graphene, but the low surface area (S_{BET} ~340 m^2 g^{-1}) limits its application for high-energy electrochemical devices.[29] By comparison, our approach is compatible with the current large-scale production method for ACs and the HPG carbon provides an ultrahigh surface area with a density (~0.47 g cm^{-3}) similar to that of commercial ACs. With a low cost of starting materials (<7−11 $/kg of HPG carbon produced, Table S2), our HPG carbon can be readily manufactured at large scale at low cost.

In summary, we have developed a scalable synthetic approach to prepare 3D porous graphitic carbon from conjugated polymer molecular framework by a one-step synthesis from low-cost starting materials. Particularly, this methodology allows production of highly graphitic carbons with ultrahigh surface area along with large pore volume and interconnected graphene-like network structures. These properties lead to exceptional electrochemical activity and high stability, with unprecedented performances in both supercapacitors and Li−S batteries. The monomer, cross-linker, and oxidation agents to make the precursor polymer can be readily changed to provide a large tunability for the final carbon morphology, surface area, and chemical composition. Our synthetic method also allows easy incorporation of metal, metal oxides, nitrides, or carbides into the carbon framework by adding metal-containing salts during the polymerization process or using it as oxidizing agent for polymerization. Therefore, this new route of making 3D porous graphitic carbons can be adapted to prepare carbon materials with desired properties for a broad range of applications.

■ ASSOCIATED CONTENT

Supporting Information

The following file is available free of charge on the ACS Publications website at DOI: 10.1021/acscentsci.5b00149.

Experimental materials and methods, more information on structure and composition analysis, electrochemical data, and cost analysis in Figures S1−S16 and Tables S1 and S2 (PDF)

■ AUTHOR INFORMATION

Corresponding Author

*E-mail: zbao@stanford.edu.

Author Contributions

‡J.W.F.T. and Z.C. contributed equally to this work

Notes

The authors declare no competing financial interest.

■ ACKNOWLEDGMENTS

This work is partially supported by the Global Climate and Energy Project (GCEP) and Preourt Institute for Energy. We acknowledge the support from the Department of Energy, through the SLAC National Accelerator Laboratory LDRD project, under Contract DE-AC02-76SF00515. Part of this work was also supported by the Assistant Secretary for Energy Efficiency and Renewable Energy, Office of Vehicle Technologies of the U.S. Department of Energy and the Battery Materials Research (BMR) Program and the SUNCAT Center for Interface Science and Catalysis, a partnership between SLAC National Accelerator Laboratory and the Department of Chemical Engineering at Stanford University.

■ REFERENCES

(1) (a) Frackowiak, E.; Béguin, F. Carbon materials for the electrochemical storage of energy in capacitors. *Carbon* **2001**, *39*, 937−950. (b) Frackowiak, E. Carbon materials for supercapacitor application. *Phys. Chem. Chem. Phys.* **2007**, *9*, 1774−1785. (c) Bruce, P. G.; Freunberger, S. A.; Hardwick, L. J.; Tarascon, J.-M. Li-O_2 and Li-S batteries with high energy storage. *Nat. Mater.* **2011**, *11*, 19−29. (d) Evers, S.; Nazar, L. F. New Approaches for High Energy Density Lithium−Sulfur Battery Cathodes. *Acc. Chem. Res.* **2012**, *46*, 1135−1143.

(2) (a) Kim, Y.-T.; Mitani, T. Competitive effect of carbon nanotubes oxidation on aqueous EDLC performance: Balancing hydrophilicity and conductivity. *J. Power Sources* **2006**, *158*, 1517−1522. (b) Gamby, J.; Taberna, P. L.; Simon, P.; Fauvarque, J. F.; Chesneau, M. Studies and characterisations of various activated carbons used for carbon/carbon supercapacitors. *J. Power Sources* **2001**, *101*, 109−116.

(3) Weinstein, L.; Dash, R. Supercapacitor carbons. *Mater. Today* **2013**, *16*, 356−357.

(4) (a) Chmiola, J.; Yushin, G.; Gogotsi, Y.; Portet, C.; Simon, P.; Taberna, P. L. Anomalous increase in carbon capacitance at pore sizes less than 1 nm. *Science* **2006**, *313*, 1760−1763. (b) Korenblit, Y.; Rose, M.; Kockrick, E.; Borchardt, L.; Kvit, A.; Kaskel, S.; Yushin, G. High-rate electrochemical capacitors based on ordered mesoporous silicon carbide-derived carbon. *ACS Nano* **2010**, *4*, 1337−1344. (c) Kajdos, A.; Kvit, A.; Jones, F.; Jagiello, J.; Yushin, G. Tailoring the pore alignment for rapid ion transport in microporous carbons. *J. Am. Chem. Soc.* **2010**, *132*, 3252−3253. (d) Li, H.-Q.; Liu, R.-L.; Zhao, D.-Y.; Xia, Y.-Y. Electrochemical properties of an ordered mesoporous carbon prepared by direct tri-constituent co-assembly. *Carbon* **2007**, *45*, 2628−2635.

(5) (a) Stoller, M. D.; Park, S.; Zhu, Y.; An, J.; Ruoff, R. S. Graphene-based ultracapacitors. *Nano Lett.* **2008**, *8*, 3498−3502. (b) Miller, J. R.; Outlaw, R. A.; Holloway, B. C. Graphene double-layer capacitor with ac line-filtering performance. *Science* **2010**, *329*, 1637−1639. (c) Raccichini, R.; Varzi, A.; Passerini, S.; Scrosati, B. The role of graphene for electrochemical energy storage. *Nat. Mater.* **2015**, *14*, 271−279. (d) Liu, J. Charging graphene for energy. *Nat. Nanotechnol.* **2014**, *9*, 739−741.

(6) (a) Chen, Z.; Ren, W.; Gao, L.; Liu, B.; Pei, S.; Cheng, H.-M. Three-dimensional flexible and conductive interconnected graphene networks grown by chemical vapour deposition. *Nat. Mater.* **2011**, *10*, 424−428. (b) El-Kady, M. F.; Strong, V.; Dubin, S.; Kaner, R. B. Laser scribing of high-performance and flexible graphene-based electrochemical capacitors. *Science* **2012**, *335*, 1326−1330. (c) Yang, X.;

DOI: 10.1021/acscentsci.5b00149
ACS Cent. Sci. 2015, 1, 68−76

Cheng, C.; Wang, Y.; Qiu, L.; Li, D. Liquid-mediated dense integration of graphene materials for compact capacitive energy storage. *Science* **2013**, *341*, 534−537. (d) Xu, Y.; Lin, Z.; Zhong, X.; Huang, X.; Weiss, N. O.; Huang, Y.; Duan, X. Holey graphene frameworks for highly efficient capacitive energy storage. *Nat. Commun.* **2014**, *5*, 4554.

(7) (a) William, S.; Hummers, R. E. O., Jr. Preparation of graphite oxide. *J. Am. Chem. Soc.* **1958**, *80*, 1339−1339. (b) Li, D.; Muller, M. B.; Gilje, S.; Kaner, R. B.; Wallace, G. G. Processable aqueous dispersions of graphene nanosheets. *Nat. Nanotechnol.* **2008**, *3*, 101−105.

(8) Zhang, J.; Zhao, Z.; Xia, Z.; Dai, L. A metal-free bifunctional electrocatalyst for oxygen reduction and oxygen evolution reactions. *Nat. Nanotechnol.* **2015**, DOI: 10.1038/nnano.2015.48.

(9) Pan, L.; Yu, G.; Zhai, D.; Lee, H. R.; Zhao, W.; Liu, N.; Wang, H.; Tee, B. C. K.; Shi, Y.; Cui, Y.; Bao, Z. Hierarchical nanostructured conducting polymer hydrogel with high electrochemical activity. *Proc. Natl. Acad. Sci. U.S.A.* **2012**, *109*, 9287−9292.

(10) (a) Solum, M. S.; Pugmire, R. J.; Jagtoyen, M.; Derbyshire, F. Evolution of carbon structure in chemically activated wood. *Carbon* **1995**, *33*, 1247−1254. (b) Jagtoyen, M.; Derbyshire, F. Activated carbons from yellow poplar and white oak by H_3PO_4 activation. *Carbon* **1998**, *36*, 1085−1097.

(11) (a) Nahil, M. A.; Williams, P. T. Pore characteristics of activated carbons from the phosphoric acid chemical activation of cotton stalks. *Biomass Bioenergy* **2012**, *37*, 142−149. (b) Raymundo-Piñero, E.; Leroux, F.; Béguin, F. A High-performance carbon for supercapacitors obtained by carbonization of a seaweed biopolymer. *Adv. Mater.* **2006**, *18*, 1877−1882. (c) Chen, J. P. High carbon yield phenolic resole. US Patent, US 2003/0135012 A1. (d) Manocha, S. M.; Patel, K.; Manocha, L. M. Development of carbon form from phenolic resin via template route. *Indian J. Eng. Mater. Sci.* **2010**, *17*, 338−342.

(12) (a) Conesa, J. A.; Sakural, M.; Antal, M. J., Jr. Synthesis of a high-yield activated carbon by oxygen gasification of macadamia nut shell charcoal in hot liquid water. *Carbon* **2000**, *38*, 839−848. (b) Dai, X.; Antal, M. J., Jr. Synthesis of a high-yield activated carbon by air gasification of macadamia nut shell charcoal. *Ind. Eng. Chem. Res.* **1999**, *38*, 3386−3395.

(13) (a) Zhu, Y.; Murali, S.; Stoller, M. D.; Ganesh, K. J.; Cai, W.; Ferreira, P. J.; Pirkle, A.; Wallace, R. M.; Cychosz, K. A.; Thommes, M.; Su, D.; Stach, E. A.; Ruoff, R. S. Carbon-based supercapacitors produced by activation of graphene. *Science* **2011**, *332*, 1537−1541. (b) Zhang, L.; Zhang, F.; Yang, X.; Long, G.; Wu, Y.; Zhang, T.; Leng, K.; Huang, Y.; Ma, Y.; Yu, A.; Chen, Y. Porous 3D graphene-based bulk materials with exceptional high surface area and excellent conductivity for supercapacitors. *Sci. Rep.* **2013**, *3*, 1408.

(14) (a) Wang, J.; Kaskel, S. KOH activation of carbon-based materials for energy storage. *J. Mater. Chem.* **2012**, *22*, 23710−23725. (b) Marsh, H.; Crawford, D.; O'Grady, T. M.; Wennerberg, A. Carbons of high surface area. A study by adsorption and high resolution electron microscopy. *Carbon* **1982**, *20*, 419−426.

(15) Berger, S. D.; McKenzie, D. R.; Martin, P. J. EELS analysis of vacuum arc-deposited diamond-like films. *Philos. Mag. Lett.* **1988**, *57*, 285−290.

(16) Ding, W.; Wei, Z.; Chen, S.; Qi, X.; Yang, T.; Hu, J.; Wang, D.; Wan, L. J.; Alvi, S. F.; Li, L. Space-confinement-induced synthesis of pyridinic- and pyrrolic-nitrogen-doped graphene for the catalysis of oxygen reduction. *Angew. Chem., Int. Ed.* **2013**, *52*, 11755−11759.

(17) Wang, X.; Zhang, Y.; Zhi, C.; Wang, X.; Tang, D.; Xu, Y.; Weng, Q.; Jiang, X.; Mitome, M.; Golberg, D.; Bando, Y. Three-dimensional strutted graphene grown by substrate-free sugar blowing for high-power-density supercapacitors. *Nat. Commun.* **2013**, *4*, 2905.

(18) Chandrasekaran, R.; Soneda, Y.; Yamashita, J.; Kodama, M.; Hatori, H. Preparation and electrochemical performance of activated carbon thin films with polyethylene oxide-salt addition for electrochemical capacitor applications. *J. Solid State Electrochem.* **2008**, *12*, 1349−1355.

(19) Kötz, R.; Carlen, M. Principles and applications of electrochemical capacitors. *Electrochim. Acta* **2000**, *45*, 2483−2498.

(20) Wu, Z.-S.; Sun, Y.; Tan, Y.-Z.; Yang, S.; Feng, X.; Müllen, K. Three-dimensional graphene-based macro- and mesoporous frameworks for high-performance electrochemical capacitive energy storage. *J. Am. Chem. Soc.* **2014**, *134*, 19532−19535.

(21) (a) Gogotsi, Y.; Simon, P. True performance metrics in electrochemical energy storage. *Science* **2011**, *334*, 917−918. (b) Stoller, M. D.; Ruoff, R. S. Best practice methods for determining an electrode material's performance for ultracapacitors. *Energy Environ. Sci.* **2010**, *3*, 1294−1301.

(22) Manthiram, A.; Fu, Y.; Su, Y.-S. Challenges and prospects of lithium−sulfur batteries. *Acc. Chem. Res.* **2012**, *46*, 1125−1134.

(23) Fu, Y.; Su, Y. S.; Manthiram, A. Highly reversible lithium/dissolved polysulfide batteries with carbon nanotube electrodes. *Angew. Chem., Int. Ed.* **2013**, *52*, 6930−6935.

(24) Yao, H.; Zheng, G.; Hsu, P. C.; Kong, D.; Cha, J. J.; Li, W.; Seh, Z. W.; McDowell, M. T.; Yan, K.; Liang, Z.; Narasimhan, V. K.; Cui, Y. Improving lithium-sulphur batteries through spatial control of sulphur species deposition on a hybrid electrode surface. *Nat. Commun.* **2014**, *5*, 3943.

(25) (a) Seh, W. Z.; Li, W.; Cha, J. J.; Zheng, G.; Yang, Y.; McDowell, M. T.; Hsu, P. C.; Cui, Y. Sulphur-TiO_2 yolk-shell nanoarchitecture with internal void space for long-cycle lithium-sulphur batteries. *Nat. Commun.* **2013**, *4*, 1331. (b) Seh, Z. W.; Yu, J. H.; Li, W.; Hsu, P. C.; Wang, H.; Sun, Y.; Yao, H.; Zhang, Q.; Cui, Y. Two-dimensional layered transition metal disulphides for effective encapsulation of high-capacity lithium sulphide cathodes. *Nat. Commun.* **2014**, *5*, 5017. (c) Pang, Q.; Kundu, D.; Cuisinier, M.; Nazar, L. F. Surface-enhanced redox chemistry of polysulphides on a metallic and polar host for lithium-sulphur batteries. *Nat. Commun.* **2014**, *5*, 4759. (d) Liang, X.; Hart, C.; Pang, Q.; Garsuch, A.; Weiss, T.; Nazar, L. F. A highly efficient polysulfide mediator for lithium-sulfur batteries. *Nat. Commun.* **2015**, *6*, 5682. (e) Song, J.; Gordin, M. L.; Xu, T.; Chen, S.; Yu, Z.; Sohn, H.; Lu, J.; Ren, Y.; Duan, Y.; Wang, D. Strong lithium polysulfide chemisorption on electroactive sites of nitrogen-doped carbon composites for high-performance lithium-sulfur battery cathodes. *Angew. Chem., Int. Ed.* **2015**, *54*, 4325−4329. (f) Zheng, S.; Yi, F.; Li, Z.; Zhu, Y.; Xu, Y.; Luo, C.; Yang, J.; Wang, C. Copper-stabilized sulfur-microporous carbon cathodes for Li-S batteries. *Adv. Funct. Mater.* **2014**, *24*, 4156−4163.

(26) Choi, N. S.; Chen, Z.; Freunberger, S. A.; Ji, X.; Sun, Y. K.; Amine, K.; Yushin, G.; Nazar, L. F.; Cho, J.; Bruce, P. G. Challenges facing lithium batteries and electrical double-layer capacitors. *Angew. Chem., Int. Ed.* **2012**, *51*, 9994−10024.

(27) (a) Zheng, G.; Zhang, Q.; Cha, J. J.; Yang, Y.; Li, W.; Seh, Z. W.; Cui, Y. Amphiphilic surface modification of hollow carbon nanofibers for improved cycle life of lithium sulfur batteries. *Nano Lett.* **2013**, *13*, 1265−1270. (b) Song, J.; Xu, T.; Gordin, M. L.; Zhu, P.; Lv, D.; Jiang, Y.-B.; Chen, Y.; Duan, Y.; Wang, D. Nitrogen-doped mesoporous carbon promoted chemical adsorption of sulfur and fabrication of high-areal-capacity sulfur cathode with exceptional cycling stability for lithium-sulfur batteries. *Adv. Funct. Mater.* **2014**, *24*, 1243−1250.

(28) Barbieri, O.; Hahn, M.; Herzog, A.; Kötz, R. Capacitance limits of high surface area activated carbons for double layer capacitors. *Carbon* **2005**, *43*, 1303−1310.

(29) Lin, J.; Peng, Z.; Liu, Y.; Ruiz-Zepeda, F.; Ye, R.; Samuel, E. L. G.; Yacaman, M. J.; Yakobson, B. I.; Tour, J. M. Laser-induced porous graphene films from commercial polymers. *Nat. Commun.* **2014**, *5*, 5714.

DOI: 10.1021/acscentsci.5b00149
ACS Cent. Sci. 2015, 1, 68−76